RESEARCH ARTICLE

CELLULAR NEUROSCIENCE

Microglia monitor and protect neuronal function through specialized somatic purinergic junctions

Csaba Cserép[1]*, Balázs Pósfai[1,2]*, Nikolett Lénárt[1], Rebeka Fekete[1,2], Zsófia I. László[2,3], Zsolt Lele[3], Barbara Orsolits[1], Gábor Molnár[4], Steffanie Heindl[5], Anett D. Schwarcz[1], Katinka Ujvári[1], Zsuzsanna Környei[1], Krisztina Tóth[1,2], Eszter Szabadits[1], Beáta Sperlágh[6], Mária Baranyi[6], László Csiba[7], Tibor Hortobágyi[8,9,10], Zsófia Maglóczky[11], Bernadett Martinecz[1], Gábor Szabó[12], Ferenc Erdélyi[12], Róbert Szipőcs[13], Michael M. Tamkun[14], Benno Gesierich[5], Marco Duering[5,15], István Katona[3], Arthur Liesz[5,15], Gábor Tamás[4], Ádám Dénes[1]†

Microglia are the main immune cells in the brain and have roles in brain homeostasis and neurological diseases. Mechanisms underlying microglia–neuron communication remain elusive. Here, we identified an interaction site between neuronal cell bodies and microglial processes in mouse and human brain. Somatic microglia–neuron junctions have a specialized nanoarchitecture optimized for purinergic signaling. Activity of neuronal mitochondria was linked with microglial junction formation, which was induced rapidly in response to neuronal activation and blocked by inhibition of P2Y12 receptors. Brain injury–induced changes at somatic junctions triggered P2Y12 receptor–dependent microglial neuroprotection, regulating neuronal calcium load and functional connectivity. Thus, microglial processes at these junctions could potentially monitor and protect neuronal functions.

Microglia are the main immunocompetent cells of the nervous system and their role in brain development and maintenance of proper neuronal function throughout life is widely recognized (*1*, *2*). Changes in microglial activity are linked with major human diseases, including different forms of neurodegeneration, stroke, epilepsy, and psychiatric disorders (*3*, *4*).

Microglia perform dynamic surveillance of their microenvironment using motile microglial processes that constantly interact with neurons (*5*, *6*). However, the molecular mechanisms of bidirectional microglia–neuron communication are unclear. To date, most studies have focused on the interactions between microglial processes and synaptic elements, including axonal boutons and dendritic spines, which have commonly been perceived as the main form of interaction between microglia and neurons (*7*, *8*). However, neurons are extremely polarized cells with a high degree of functional independence concerning metabolism and signal integration in their dendritic and axonal compartments (*9*–*11*). The large-scale structure of neurons (i.e., their cell body and axonal or dendritic branches) in the brain is relatively stable under most conditions. In comparison, small synaptic structures such as dendritic spines and axonal boutons are often distant from neuronal cell bodies and are highly dynamic. Therefore, the interactions between microglia and synapses may not fully explain how microglia are capable of monitoring and influencing the activity of neurons or how early events of cellular injury in the perisomatic compartment are detected. This may be particularly relevant for the migration and differentiation of neural precursors, cell survival and programmed cell death, adult neurogenesis, and the phagocytosis of damaged neuronal cell bodies (*12*–*15*). It is not understood how microglia could monitor neuronal status over years or even decades and discriminate salvageable neurons from irreversibly injured cells mainly on the basis of changes occurring at distant synaptic structures.

To understand the possible mechanisms of effective communication between microglia and neurons, we tested the hypothesis that specialized junctions on neuronal cell bodies may support the dynamic monitoring and assistance of neuronal function by microglia.

Microglial processes contact specialized areas of neuronal cell bodies in mouse and human brains

To visualize microglia together with cortical neurons and to study microglia–neuron interactions in the intact brain in real time, $CX3CR1^{+/GFP}$ microglia reporter mice were electroporated in utero with *pCAG-IRES-tdTomato* plasmid (fig. S1A). In vivo two-photon (2P) imaging revealed microglial processes contacting the cell bodies of cortical layer 2 to 3 neurons in the adult brain (Fig. 1, A and B, and movie S1). Microglial processes preferentially returned to the same areas on the neuronal soma (observed in 23 neurons out of 28 from 3 mice). The average lifetime of somatic microglia–neuron contacts was 25 min; some contacts persisted for >1 hour (fig. S1B), whereas dendritic contacts had a significantly shorter lifetime of 7.5 min (Fig. 1C; $p = 0.00035$; $n = 26$ contacts from 3 mice), similar to that reported for synaptic contacts (*16*). Post hoc confocal laser scanning microscopy (CLSM) and electron microscopic analysis further validated the direct interaction between microglial processes and the cell bodies of cortical pyramidal neurons (Fig. 1D and fig. S1, C and D), which we named somatic microglial junction. Similar interactions were present on well-characterized interneuron populations, namely type 3 vesicular glutamate transporter–positive ($vGluT3^+$) and parvalbumin-expressing (PV^+) cells in the neocortex and the hippocampus (fig. S1E). Somatic microglia–neuron junctions were also observed in the human neocortex (Fig. 1E). Somatic microglial junctions were present on 93% of cortical pyramidal neurons, 95% of $vGluT3^+$ neurons, and 89% of PV^+ interneurons in mice ($n = 443$ cells from 4 mice). Despite the well-established microglial regulation of neuronal synapses, only 9% of glutamate-releasing and 11% of γ-aminobutyric acid (GABA)–releasing synapses were associated with microglial processes (Fig. 1F and fig. S1F; $n = 1183$ synapses from 4 mice). Eighty-seven percent of neurons in the human neocortex received microglial contact with their cell body (Fig. 1, E and F; n = 170 cells from 3 patients). We also tested the possible presence of somatic microglial junctions in subcortical areas. Ninety-eight percent of neurons in the caudate putamen, 91% of neurons in the nucleus reticularis gigantocellularis, and 96% of neurons in the medial septum were contacted by microglial processes

[1]Momentum Laboratory of Neuroimmunology, Institute of Experimental Medicine, Budapest, Hungary. [2]Szentágothai János Doctoral School of Neuroscience, Semmelweis University, Budapest, Hungary. [3]Momentum Laboratory of Molecular Neurobiology, Institute of Experimental Medicine, Budapest, Hungary. [4]MTA-SZTE Research Group for Cortical Microcircuits of the Hungarian Academy of Sciences, Department of Physiology, Anatomy and Neuroscience, University of Szeged, Szeged, Hungary. [5]Institute for Stroke and Dementia Research, Ludwig-Maximilians-University, Munich, Germany. [6]Laboratory of Molecular Pharmacology, Institute of Experimental Medicine, Budapest, Hungary. [7]MTA-DE Cerebrovascular and Neurodegenerative Research Group, Department of Neurology, University of Debrecen, Debrecen, Hungary. [8]Institute of Pathology, Faculty of Medicine, University of Szeged, Szeged, Hungary. [9]Department of Old Age Psychiatry, Institute of Psychiatry, Psychology and Neuroscience, King's College London, London, UK. [10]Centre for Age-Related Medicine, SESAM, Stavanger University Hospital, Stavanger, Norway. [11]Human Brain Research Laboratory, Institute of Experimental Medicine, Budapest, Hungary. [12]Medical Gene Technology Unit, Institute of Experimental Medicine, Budapest, Hungary. [13]Institute for Solid State Physics and Optics of Wigner RCP, Budapest, Hungary. [14]Department of Biomedical Sciences, Colorado State University, Fort Collins, Colorado, USA. [15]Munich Cluster for Systems Neurology (SyNergy), Munich, Germany.
*These authors contributed equally to this work.
†Corresponding author. Email: denes.adam@koki.mta.hu

(n = 268 cells from 2 mice). Thus, these contacts are evolutionary conserved and present in all main areas of the brain.

Microglia at somatic junctions may sense changes in neuronal state through signals released by exocytosis. In neurons, clustered Kv2.1 proteins are well known to provide exocytotic surfaces by anchoring vesicle fusion molecules to the neuronal membrane (*17*, *18*). Furthermore, both Kv2.1 and Kv2.2 proteins are involved in forming endoplasmic reticulum (ER)–plasma membrane (PM) junctions (membrane-trafficking hubs) and in anchoring intracellular organelles to the neuronal PM (*19*). Microglia contacted neuronal somatic membranes at sites of Kv2.1 and Kv2.2 clustering (Fig. 1G). The integrated density of Kv2.1 signal at these sites was 96% higher and the density of Kv2.2 signal was 254% higher compared with those without microglial contacts (Fig. 1H; $p < 0.0001$ in both cases; n = 114 and n = 107, respectively, from 3 mice). Eighty-seven percent of all microglia–neuron contacts expressed both types of clusters, 6.3% expressed only Kv2.1 clusters, 4.5% only Kv2.2 clusters, and only 1.8% of contacts were void of any Kv clusters (Fig. 1I; n = 111 contacts from 2 mice). Furthermore, 99% of neocortical and 94% of hippocampal CA1-region neurons expressed both Kv2.1 and Kv2.2 channels at the cellular level (fig. S2, A to C). The spatial association between Kv2.1 clusters and microglial processes was also observed on human cortical neurons (fig. S1, G and H; n = 21 cells). Because Kv2.1 clusters are implicated in a large number of cellular processes involved in cell-to-cell

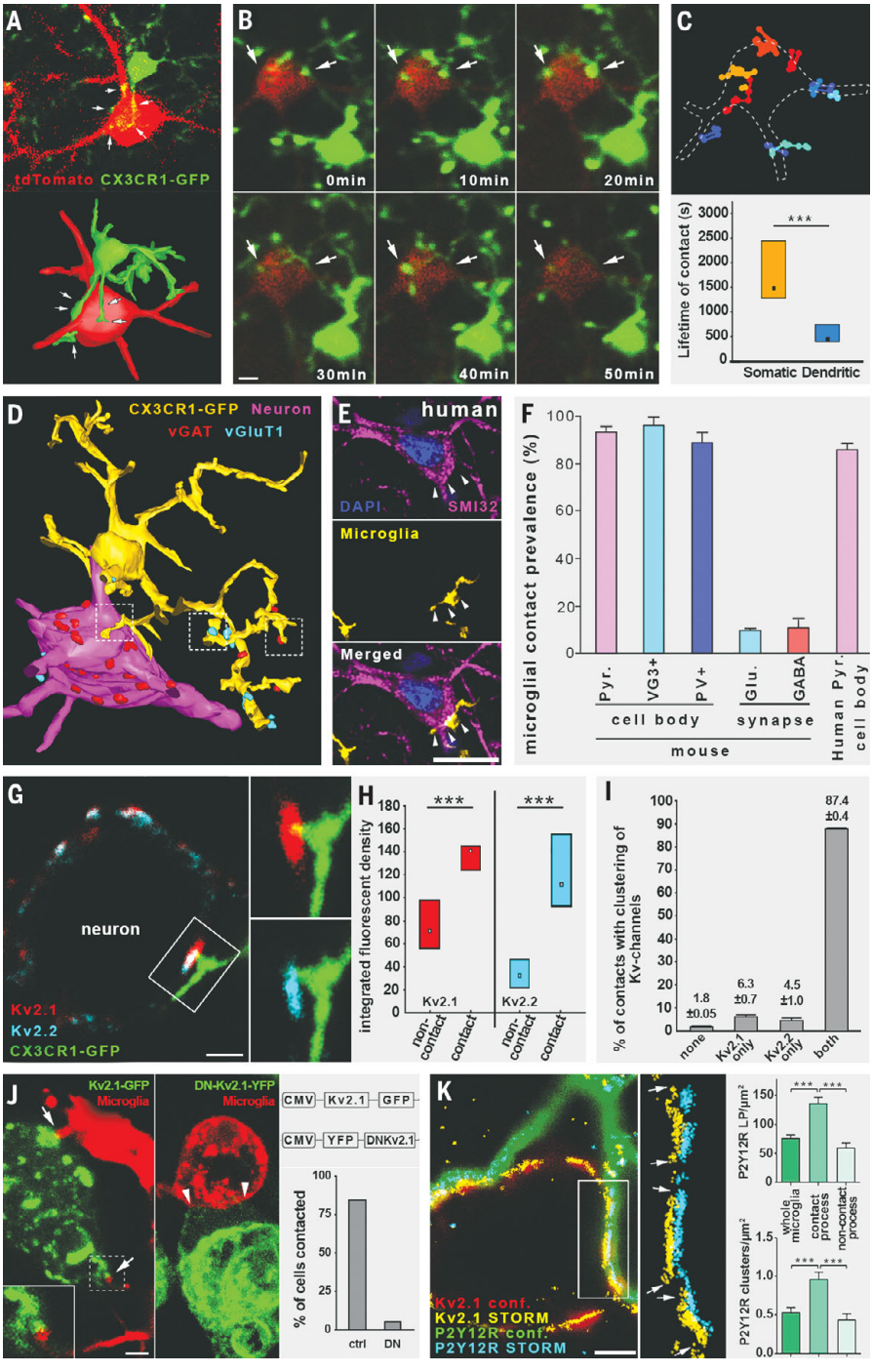

Fig. 1. Microglia contact specialized areas of neuronal cell bodies in the mouse and the human brain. (**A**) Single image plane (upper panel) and 3D reconstruction (lower panel) from an in vivo 2P *Z*-stack showing a neocortical neuron (red) being contacted by microglial processes (green). (**B**) In vivo 2P time-lapse imaging showing temporal dynamics of microglia–neuron contacts. (**C**) Analyzed trajectories of microglial processes contacting the neuron in (B). The lifetimes of somatic contacts were significantly longer than those of dendritic contacts. (**D**) 3D reconstruction from high-resolution CLSM *Z*-stack showing that microglial processes (yellow) contact GABA-releasing (red) and glutamate-releasing (cyan) boutons as well as the neuronal cell body (Kv2.1 labeling, magenta). (**E**) CLSM images showing P2Y12 receptor$^+$ microglial processes (yellow) contacting an SMI32$^+$ neuronal cell body (magenta) in human neocortex. (**F**) Quantitative analysis of contact prevalence between microglial processes and different neuronal elements confirming that microglia contact most neuronal cell bodies independently from neurochemical identity, whereas only a small fraction of synapses receive microglial contact. (**G**) CLSM image showing a neuronal cell body contacted by a microglial process at a Kv2.1 to Kv2.2 cluster. (**H**) The integrated fluorescent density of both Kv2.1 and Kv2.2 signal is significantly higher within the contact site than elsewhere. (**I**) Most microglia–neuron junctions expressed both Kv2.1 and Kv2.2 clusters. (**J**) Microglial processes contact Kv2.1-transfected HEK cells at the clusters, but not those transfected with a dominant-negative mutant. (**K**) Overlaid images showing microglial P2Y12 receptor (green for CLSM and cyan for STORM) and neuronal Kv2.1 (red for CLSM and yellow for STORM) clusters overlapping. Arrows show borders of Kv2.1 clusters. P2Y12 receptor clustering depends on the contact with neuronal cell body. Bar graphs show STORM localization point (LP) density (top) and density of identified P2Y12 receptor clusters (bottom) on different parts of microglia (for statistics, see table S1). P2Y12R, P2Y12 receptor. For statistical details, see the supplementary text for Fig. 1 and table S1.

communication, we focused on Kv2.1 in our further experiments. Kv2.1 hot spots appeared to define preformed neuronal microdomains because Kv2.1 clusters remained unaltered after selective elimination of microglia by PLX5622 (fig. S1, I and J; 4.71 clusters per cross-section in control versus 6.64 clusters per cross-section in depleted; $n = 59$ cells from 4 mice). To test the functional involvement of Kv2.1 clusters in the formation of somatic junctions, we developed a dominant-negative Kv2.1 mutant construct, DNKv2.1. This construct could not integrate into the PM and blocked the forward trafficking of any endogenous Kv2 proteins that may be expressed. We transfected human embryonic kidney (HEK) 293 cells, which naturally lack Kv2.1 protein (*20*), with fluorescent protein–coupled Kv2.1 or DNKv2.1 constructs and cocultured these with microglia. Microglial processes contacted Kv2.1-transfected HEK cells preferentially at Kv2.1 clusters and did not contact the DNKv2.1-transfected HEK cells (Fig. 1J and movie S2). Eighty-four percent of Kv2.1-transfected HEK cells received microglial process contacts (97% of these contacts arrived onto Kv2.1 clusters), whereas only 5.4% of DNKv2.1-transfected HEK cells received process contacts ($n = 75$ cells from 3 experiments). Thus, cell surface expression and clustering of Kv2.1 proteins is sufficient to induce contact formation by microglial processes.

Activity-dependent exocytotic adenosine 5′-triphosphate (ATP) or adenosine 5′-diphosphate (ADP) release takes place from neuronal cell bodies under physiological conditions (*21*, *22*). ATP (ADP) is a major chemoattractant for microglial processes through the microglial purinoceptor P2Y12 receptor (*5*, *23*). We thus asked whether signaling through P2Y12 receptor was also essential for microglia–neuron interactions at these somatic junctions. In fact, all microglia, but no other cells in the brain, including perivascular macrophages, were found to be P2Y12 receptor positive (fig. S3), including their processes recruited to somatic junctions (fig. S3B). The restriction of P2Y12 receptor expression to microglia within the brain agrees with results of earlier single-cell transcriptomics studies (*24*, *25*).

To investigate the nanoscale architecture of P2Y12 receptors at somatic microglia–neuron junctions, we used correlated CLSM and STORM superresolution microscopy, which enables the precise assessment of P2Y12 receptor and Kv2.1 clusters at 20-nm lateral resolution (*26*). P2Y12 receptors formed dense clusters on microglial processes at somatic junctions directly facing neuronal Kv2.1 clusters (Fig. 1K). Unbiased cluster analysis revealed that P2Y12 receptor localization point density and cluster density were both significantly higher on microglial processes inside the junctions than on processes outside the junctions or on the whole microglial cell (Fig. 1K and fig. S2D; for detailed statistics and numbers, see table S1). Furthermore, somatic contact–dependent clustering of P2Y12 receptors occurred on both pyramidal cells and interneurons (fig. S2E; for detailed statistics and numbers, see table S1). Contact-dependent molecular clustering, however, could not be observed in the case of the microglial calcium-binding protein Iba1 (fig. S2F). Contact-dependent P2Y12 receptor clustering was specific to somatic junctions, and immunogold density was 62% lower on microglial membranes contacting boutons than on those contacting somata (fig. S2G; $p = 0.0002$; $n = 26$ contacts from 3 mice). Thus, we suggest the existence of a functionally specialized yet ubiquitous communication site between P2Y12 receptor–positive microglial processes and neuronal cell bodies.

Somatic microglia–neuron junctions have a specific nanoarchitecture and molecular fingerprints

To further investigate the ultrastructural features of somatic microglia–neuron junctions, we performed transmission electron microscopy and high-resolution electron tomography with three-dimensional (3D) reconstruction. P2Y12 receptor immunogold labeling confirmed the formation of direct junctions between microglial processes and neuronal somata both in mice (Fig. 2A) and in postmortem human brain tissue (fig. S4A). Microglia–neuron junctions were composed of closely apposed mitochondria, reticular membrane structures, intracellular tethers, and associated vesicle-like membrane structures within the neuronal cell body (Fig. 2A). 3D electron tomography confirmed this nanoarchitecture in neurons (Fig. 2B and movies S3 and S4). These morphological features were not observed in perisomatic boutons contacted by microglia. Furthermore, automated 3D analysis of tomographic volumes showed that P2Y12 receptor density negatively correlated with the distance between microglial and neuronal membranes within the junctions (Fig. 2, C and D, and fig. S4C; $p < 0.001$; $n = 13{,}055$ points from 3 contacts). We also compared P2Y12 receptor density between microglial membrane surfaces establishing junctions with neuronal somata and adjacent surfaces (within a few micrometers) that contacted boutons or other neuronal elements. We detected a significantly higher P2Y12 receptor density at microglial membranes directly contacting neuronal cell bodies (Fig. 2E and movie S5; $p = 0.00115$; $n = 24$ surfaces). This suggests an important role for purinergic signaling in the formation of somatic microglia–neuron junctions.

We also observed discrete intercellular structures resembling cell-adhesion molecules in the extracellular space that connected the membranes of microglia and neuronal cell bodies (average length 23.5 ± 3.1 nm; $n = 89$ from 3 mice; fig. S4B). This falls in the range of the size of integrins expressed by microglia (*27*, *28*) or the width of immunological synapses between peripheral immune cells (*29*). Mitochondria-associated membranes (MAMs, average distance: 19.5 nm; $n = 104$ from 3 mice; fig. S4B) were observed (*30*) and discrete tethers between mitochondria and MAMs were also visible (movie S4).

We hypothesized that mitochondrial ATP production and changes in neuronal activity could trigger microglial process recruitment. Thus, we investigated the possible enrichment of neuronal mitochondria at microglial junctions on a large sample size using an unbiased, semiautomatic analysis of the outer mitochondrial membrane protein TOM20. TOM20 immunofluorescent intensity was 420% higher at somatic junctions compared with adjacent areas (Fig. 2, F and G; $p < 0.001$; $n = 14$ contacts from 2 mice), confirming the strong accumulation of neuronal mitochondria at the somatic junctions.

TOM20-positive vesicles were observed between mitochondria and the neuronal membrane in addition to TOM20-negative vesicles (Fig. 2H and fig. S4, E and F). This may suggest trafficking and possible exocytosis of mitochondria-derived vesicles (*31*) at somatic microglial junctions. Mitochondria-derived vesicles (MDVs) often integrate into the endolysosomal pathway (*31*), and these vesicles are positive for the lysosomal marker LAMP1 (*32*). Indeed, LAMP1-positive puncta were closely associated with 83.3% of all Kv2.1 clusters at somatic junctions (fig. S4G; $n = 72$ contacts from 2 mice), suggesting the release of MDVs and lysosomal content at these junctions.

Kv2.1–immunogold clusters were tightly associated with the observed neuronal structures (i.e., closely apposed mitochondria, MAMs, ER, vesicle-like structures, cytoplasmic densities) within these junctions (fig. S4D). Similarly to our CLSM results (fig. S1I), Kv2.1 nanoclustering was not affected by the absence of microglia (fig. S4D). These structures may function as mitochondria-related signaling hubs in neurons that microglia can recognize. Vesicular release of mitochondria-derived ATP from neurons may occur in a vesicular nucleotide transporter (vNUT)–dependent manner (*33*, *34*). Indeed, vNUT signal intensity was 2.5 times higher in the vicinity of the neuronal membranes at somatic microglia–neuron junctions compared with areas outside the junctions (Fig. 2I; $p = 0.002$; $n = 15$ contacts from 2 mice). Neuronal vNUT labeling was concentrated between mitochondria and the microglia-contacted neuronal membranes (Fig. 2J).

Kv2.1 or vNUT signal was not present in perisomatic axon terminals (GABA-releasing synaptic boutons), including those contacted by microglial processes (fig. S4, H and I; $n = 220$ boutons for Kv2.1 and $n = 194$ boutons for vNUT from 2 mice), confirming again that

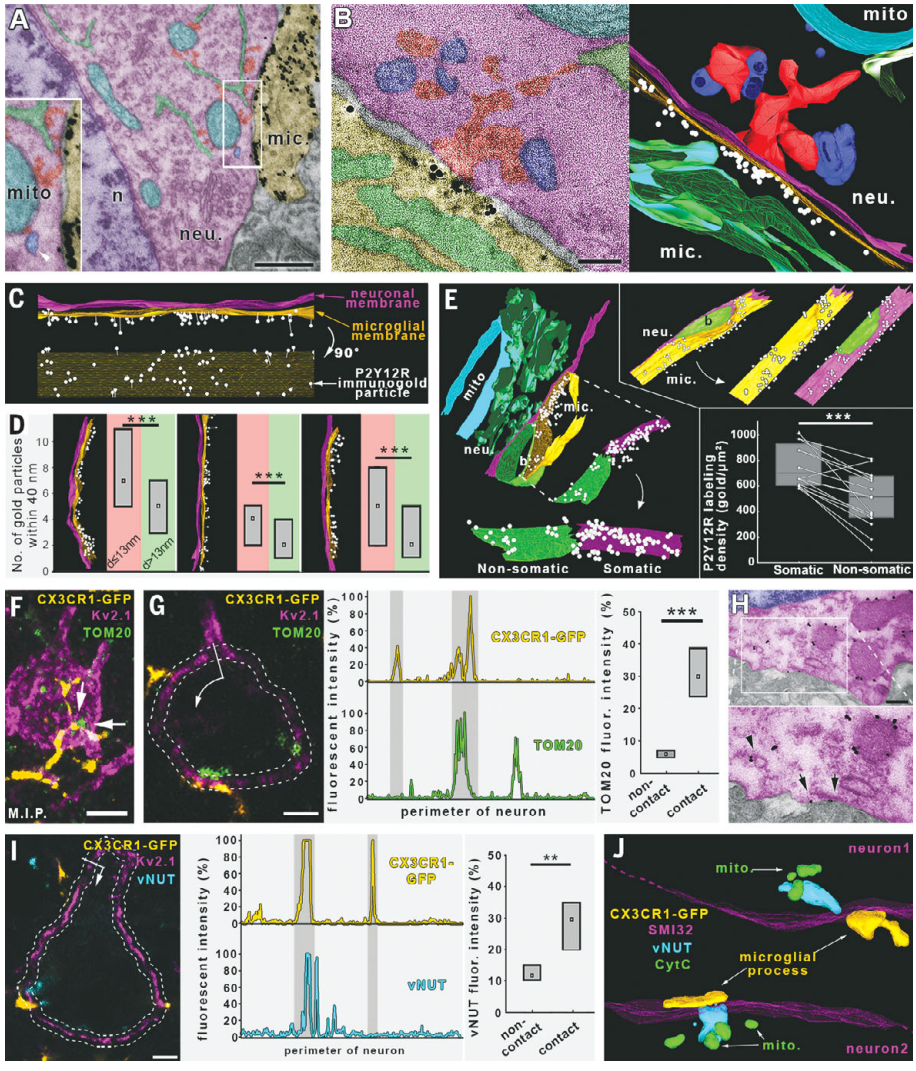

Fig. 2. Microglia–neuron junctions have a specialized nanoarchitecture and molecular machinery optimized for purinergic cell-to-cell communication. (**A**) Transmission electron micrograph showing the area of the neuronal cell body (neu.) contacted by a P2Y12 receptor–immunogold (black grains)–labeled microglial process (mic.). The junction has a specific ultrastructure with closely apposed mitochondria (mito., cyan), reticular membrane structures (green), and intracellular tethers (red). A mitochondria-associated vesicle (blue, marked by white arrowhead) is also visible. The nucleus (n) of the neuron is purple. (**B**) A 0.5-nm-thick virtual section of an electron tomographic volume (left) and 3D model (right) showing the special nanoarchitecture of a somatic microglia–neuron junction [colors represent the same structures as in (A)]. Note the specific enrichment of P2Y12 receptor labeling at the core of the junction. (**C** and **D**) P2Y12 receptor density negatively correlates with the distance between microglial and neuronal membranes within the junctions. (**E**) P2Y12 receptor density is highest at those surfaces of microglial processes that are in direct contact with the neuronal cell bodies (P2Y12 receptor labeling is white; b, bouton). (**F**) CLSM maximal intensity projection (M.I.P.) showing microglial processes (yellow) contacting neuronal somata (magenta) with adjacent mitochondria (green). (**G**) Neuronal mitochondria are enriched at microglial junction sites. (**H**) Transmission electron micrographs showing TOM20-immunogold labeling in neocortical neurons. Immunogold labeling (black grains) is specifically associated with outer mitochondrial membranes, whereas TOM20-positive vesicles can also be observed (arrowheads). Some immunogold particles can be found on the PM of the neurons (arrows), suggesting the exocytosis of mitochondria-derived vesicles. (**I**) vNUT-labeled vesicles are enriched at microglial junction sites. (**J**) 3D reconstruction of high-resolution confocal *Z*-stack showing parts of two neuronal cell bodies (magenta), both contacted by microglial processes (yellow). The vNUT signal (cyan) was concentrated between the junctions and closely positioned mitochondria (green). For statistical details, see the supplementary text for Fig. 2.

these molecular fingerprints were associated with somatic microglia–neuron junctions.

Physiological microglia–neuron communication at somatic junctions is P2Y12 receptor dependent and linked with neuronal mitochondrial activity

Next, we aimed to test whether microglial process recruitment to somatic junctions was functionally linked with the activity of mitochondria in neurons. To this end, CX3CR1$^{+/GFP}$ mice were electroporated in utero with the mitochondria-targeted *CAG-Mito-R-Geco1* reporter construct (fig. S5A). Again, we observed the involvement of somatic mitochondria in microglial junctions (Fig. 3A). In vivo 2P imaging was performed to monitor microglial process recruitment to neuronal mitochondria in the cerebral cortex (Fig. 3B). As expected, recruited microglial processes came into close apposition with neuronal mitochondria. These processes stayed in the vicinity of neuronal mitochondria for ~29 min in vivo (Fig. 3B and movie S6; n = 25 contacts on 19 neurons from 3 mice, median value), closely matching the value measured in tdTomato-electroporated mice (Fig. 1C). To study the functional relationship between microglial junction formation and activity of neuronal mitochondria, we assessed intracellular changes of the metabolic electron carrier nicotinamide adenine dinucleotide (NADH) (*35*) in coronal slices of visual and somatosensory cortices from CX3CR1$^{+/GFP}$ mice. Intracellular NADH fluorescence showed a granular pattern, indicating a mitochondrial NADH source. Indeed, the NADH signal colocalized with the *Mito-R-Geco1* signal, confirming its mitochondrial origin (fig. S5C). To search for somatic junction formation, we performed 2P imaging, which allowed us to track the movement of microglial processes and monitor cytosolic NADH in viable layer 2/3 neurons simultaneously (fig. S5D). We detected apparent increases in NADH intrinsic fluorescence (Fig. 3, C and E; p = 0.024; n = 10 cells) in parallel with the formation of somatic microglial junctions. By contrast, we found no changes in the mean intrinsic NADH fluorescence detected at neuronal somata contacted by microglial processes in P2Y12 receptor$^{-/-}$ tissue (Fig. 3, D and E; p = 0.3; n = 11 cells). Thus, microglial process recruitment to somatic junctions is linked to the metabolic activity of neuronal mitochondria through a P2Y12 receptor–dependent mechanism.

The molecular machinery and intercellular interactions identified above suggested the involvement of purinergic signaling in these somatic junctions. To test whether neuronal somata could release ATP at these sites, we conducted a series of in vitro experiments. Quinacrine-labeled ATP-containing vesicles localized between neuronal mitochondria and

neuronal membranes were present at sites where microglial processes contacted neuronal Kv2.1 clusters in microglia–neuron cocultures (Fig. 3F). Quinacrine labeling also colocalized with vNUT signal (Fig. 3F), as previously demonstrated for neurons (*33*).

Next, we tested whether neuronal activity could release ATP-containing vesicles from neuronal cell bodies. KCl (40 mM) stimulation induced a rapid membrane depolarization and calcium influx in cultured neurons (fig. S5E; n = 23 cells for FluoVolt measurements, n = 20 cells for Rhod3 measurements). CLSM in vitro time-lapse imaging confirmed that quinacrine-labeled (ATP-containing) vesicles were released from neuronal cell bodies after KCl stimulation (Fig. 3, G and H; 880% increase in release events after KCl versus a 27% decrease after vehicle; n = 13 cells). Size analysis confirmed that the smaller vesicles were released [Fig. 3I; median diameter of released vesicles was 0.37 μm and that for retained vesicles was 0.59 μm (n = 118 puncta), similar to previous reports (*33*)]. The larger vesicles were identified as mitochondria by their uniform TOM20 labeling (Fig. 3I; median diameter of vesicle labeling was 0.45 μm and that for mitochondrial labeling was 1.2 μm; n = 83 puncta).

Next, we applied high-sensitivity high-performance liquid chromatography (HPLC) to detect the levels of released ATP in the medium (Fig. 3J). KCl induced a robust ATP release in cultured neurons (p = 0.0218; n = 11), which was not inhibited by a mixture of the synaptic calcium-channel blockers ω-agatoxin and ω-conotoxin (p = 0.6532; n = 11), but was almost completely inhibited by the L-type calcium-channel blocker nimodipine [known to be important for somatic vesicular release

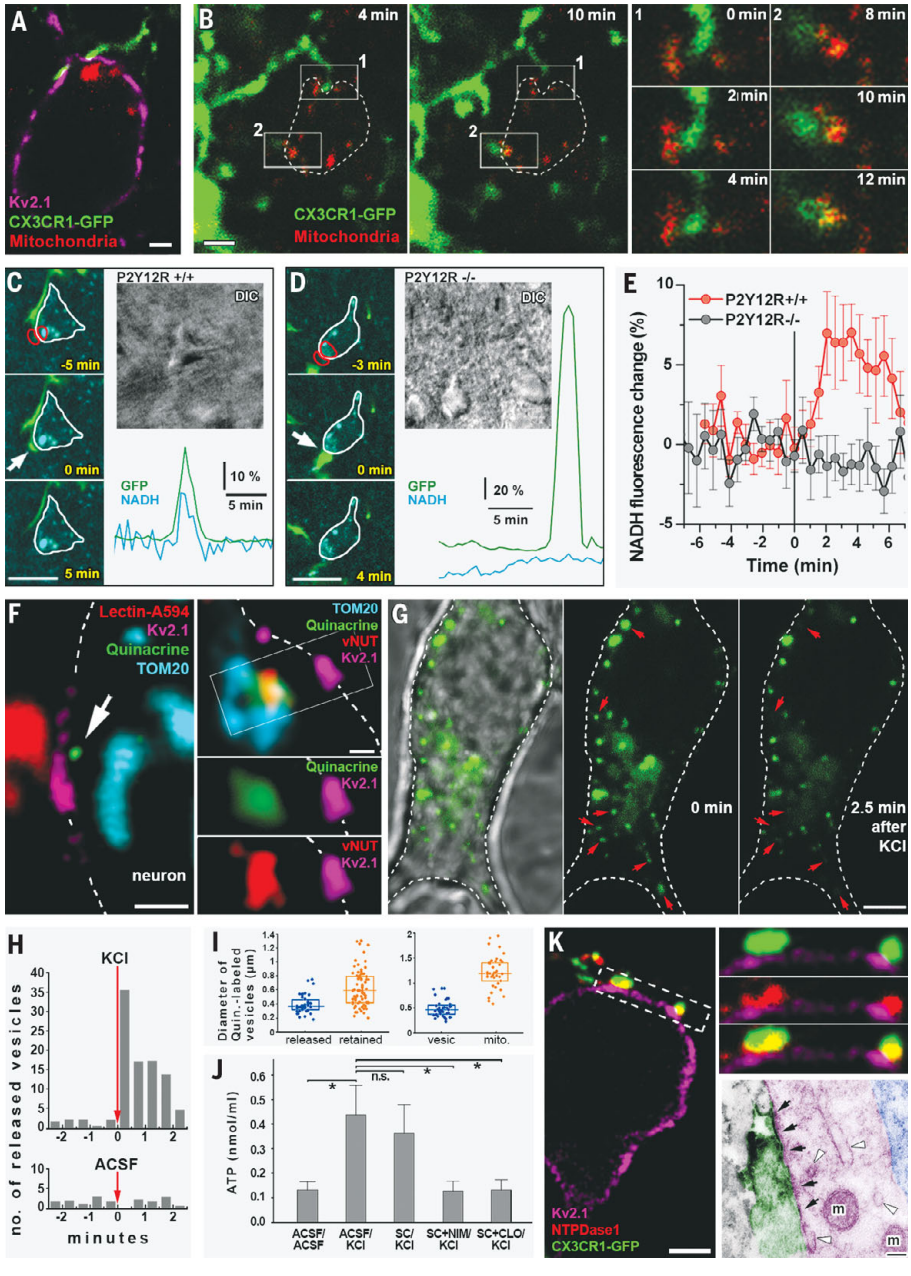

Fig. 3. Neuronal mitochondrial activity and purinergic signaling are involved in microglia–neuron communication. (**A**) CLSM image showing a microglial process (green) contacting Kv2.1 clusters (magenta) on a neuronal soma in the vicinity of a mitochondrion (Mito-R-Geco1, red) in a perfusion-fixed brain. (**B**) In vivo 2P imaging of CX3CR1$^{+/GFP}$ mice in utero electroporated with CAG-Mito-R-Geco1 construct. Dashed line shows the outline of the neuron. Green microglial processes touch the neuronal cell body where somatic mitochondria are present. Regions of interest 1 and 2 are enlarged to show the development of somatic junctions. (**C** and **D**) Representative samples from time-lapse imaging of microglia showing processes extending and contacting neuronal soma in CX3CR1$^{+/GFP}$/P2Y12 receptor$^{+/+}$ (C) and CX3CR1$^{+/GFP}$/P2Y12 receptor$^{-/-}$ (D) mice. White arrow indicates the contact site of microglia. Differential interference contrast (DIC) images of the imaged neurons and the fluorescence signal of GFP (green) and NADH (dark cyan) of red outlined areas are shown. (**E**) Average (and standard deviation) of NADH intrinsic fluorescence of all neurons in P2Y12 receptor$^{+/+}$ (red, n = 10) and P2Y12 receptor$^{-/-}$ (black, n = 11) mice. (**F**) CLSM image showing microglial process contacting a neuronal Kv2.1 cluster with closely apposed quinacrine-labeled ATP-containing vesicle and closely localized neuronal mitochondria. Quinacrine labeling colocalizes with the vNUT signal. (**G**) Images from CLSM in vitro time-lapse imaging showing that quinacrine-labeled ATP-containing vesicles (green) are released (red arrows) from the neuronal cell body (white dashed outline) after KCl stimulation (M.I.P. of Z stack, 2.5 μm). (**H**) Number of released quinacrine-positive vesicles plotted as a function of time after KCl or vehicle treatment. (**I**) Size distribution of quinacrine-labeled puncta. The smaller ones (vesicles) tend to be released and the larger ones (mitochondria) are retained. (**J**) KCl induces a robust ATP release in cultured neurons, which could not be inhibited by a mixture of the synaptic calcium-channel blockers ω-agatoxin and ω-conotoxin (SC), but was almost completely inhibited by the L-type calcium-channel blocker nimodipine (NIM) or the vNUT inhibitor clodronate (CLO). (**K**) CLSM image showing robust NTPDase1 expression on microglial processes within the somatic junctions. Electron microscopic insert shows NTPDase1-labeled (dark precipitate) microglial process contacting the neuronal cell body. Neuronal mitochondria (m), vesicles, and membrane structures (white arrowheads) are closely apposed to the contact site (black arrows) where NTPDase1 is expressed on the microglial membrane. For statistical data, see the supplementary text for Fig. 3.

(*36*); $p = 0.0271$; $n = 10$] or the vNUT inhibitor clodronate ($p = 0.0284$; $n = 10$). These data confirmed the presence of an activity-dependent somatic ATP release from neurons. Because the main ligand for microglial P2Y12 receptors is ADP, we tested the possible presence of nucleosidase expression at microglia–neuron contacts. Using CLSM and electron microscopy, we found robust NTPDase1 expression on 99.6% of all microglial processes within the somatic junctions (Fig. 3K; $n = 275$ contacts from 2 mice). Thus, neuron-derived ATP can readily be converted into ADP and sensed by microglia right within the somatic junctions.

Because microglial processes are in a position at the somatic junctions to sense neuronal activity, we further explored the signaling mechanisms at these sites in vivo using 2P imaging in CX3CR1$^{+/GFP}$ microglia reporter mice that were electroporated in utero with the neuronal reporter *pCAG-IRES-tdTomato* (Fig. 4, A and B). Intra–cisterna magna administration of the potent and selective P2Y12 receptor inhibitor PSB0739 (PSB) reduced somatic junction lifetime by 45% but did not affect the lifetime of dendritic microglia–neuron contacts (Fig. 4C, control somata versus PSB somata; $p = 0.0331$; $n = 40$). We also tested synapse density after acute intra–cisterna magna administration of vehicle (control) or PSB. PSB treatment did not alter neocortical synapse numbers (fig. S6G; 0.353 synapses/μm^2 in control somata and 0.352 synapses/μm^2 in PSB-injected somata; $n = 423$ appositions from 4 animals). Because the maintenance of somatic microglia–neuron junctions depends on physiological P2Y12 receptor function, we tested whether microglia would react directly to changes in neuronal activity. We induced neuronal activation by using the chemogenetic DREADD (designer receptor exclusively activated by designer drug) approach. pAAV carrying the hSyn-hM3D(Gq)-mCherry construct was injected into the cerebral cortex of P2Y12 receptor$^{+/+}$ and P2Y12 receptor$^{-/-}$ mice that had been crossed with CX3CR1$^{+/GFP}$ mice to visualize microglial responses in the presence or absence of P2Y12 receptor signaling (fig. S5, F and G). After intraperitoneal injection of clozapine-*N*-oxide (CNO) to induce hM3D(Gq)-DREADD activation, we observed a 234% increase in neuronal cFos signal compared with vehicle treatment (fig. S5H; $p < 0.001$; $n = 100$), confirming a specific and robust neuronal activation.

Chemogenetic neuronal activation resulted in an increased microglial process coverage of the soma of DREADD- and cFos-coexpressing neurons in P2Y12 receptor$^{+/+}$ mice (Fig. 4D; 243% of control, $p = 0.0139$; $n = 101$ neurons from 8 mice), but not in P2Y12 receptor$^{-/-}$ mice (Fig. 4E; 133% of control, $p = 0.7497$; $n =$ 85 neurons from 6 mice). We also tested the effect of acute central pharmacological blockade of microglial P2Y12 receptors (Fig. 4F) and found that PSB injected intra–cisterna magna completely abolished the neuronal activity–induced increase in microglial process coverage (Fig. 4G; 72.34% lower process coverage in CNO+PSB than in CNO+vehicle, $p < 0.001$; $n =$ 124 neurons from 6 mice). Thus, microglia dynamically react to changes in neuronal activity at somatic microglia–neuron junctions in a P2Y12 receptor–dependent manner, leading to a rapid increase of somatic coverage by microglial processes.

Microglia protect neurons after acute brain injury in a P2Y12 receptor–dependent manner through altered somatic junctions

Because somatic microglia–neuron junctions were abundant in the healthy brain, we next investigated whether these morphofunctional communication sites were altered in response to brain injury. Microglia are known to respond rapidly to changes in neuronal activity in the boundary zone of the infarct after stroke (*37*). Thus, we performed experimental stroke and delineated the evolving penumbra on the basis of the metabolic activity of the tissue as assessed by the redox indicator tetrazolium chloride coregistered with the immunofluorescent signal for MAP2 and microglia

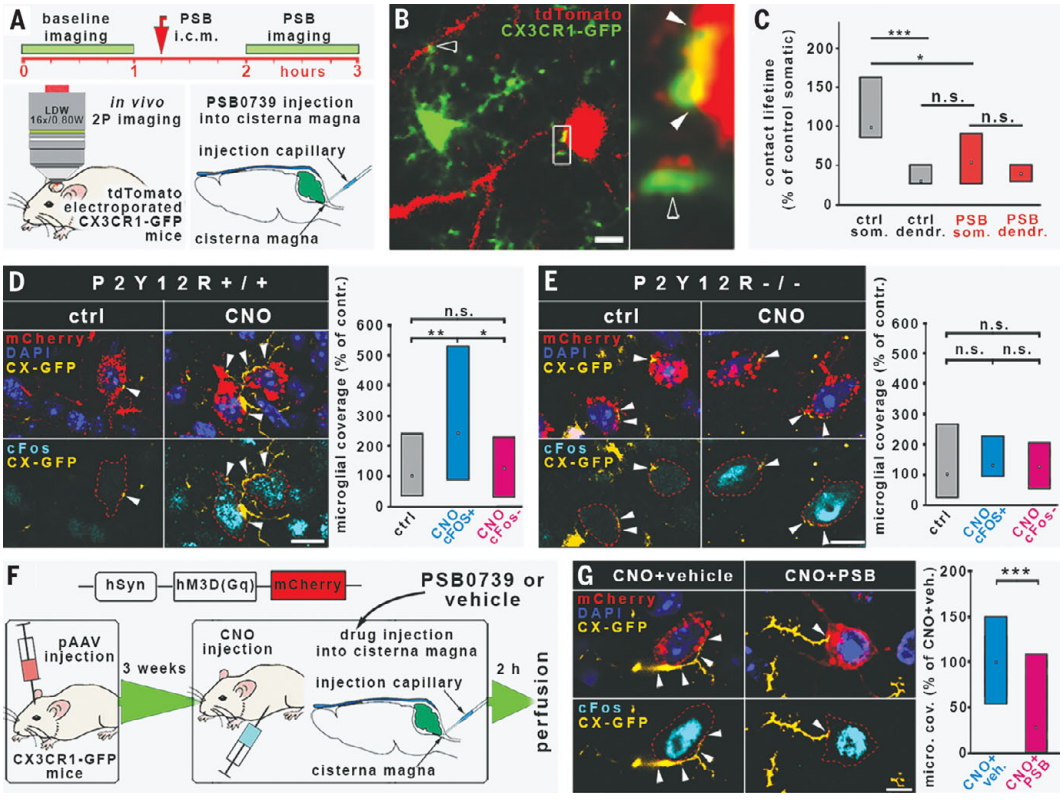

Fig. 4. Physiological microglia–neuron communication at the somatic junction site is P2Y12 receptor dependent. (**A**) Outline of acute P2Y12 receptor–blockade experiments. i.c.m., intra–cisterna magna. (**B**) CLSM images showing examples of the recorded microglia–neuron contacts. Empty arrowheads point to dendritic contacts and full arrowheads mark somatic junctions. (**C**) Acute intra–cisterna magna administration of PSB significantly reduced somatic junction lifetime, but did not affect the lifetime of dendritic microglia–neuron contacts. n.s., not significant. (**D**) Neuronal activity induced a robust elevation of microglial process coverage of neuronal cell bodies in CNO-treated animals but not in DREADD^{+}/cFos^{-} cells. (**E**) CNO-triggered neuronal activity could not induce an elevation of microglial process coverage of neuronal cell bodies in P2Y12 receptor$^{-/-}$ mice. (**F**) Outline of combined chemogenetic and acute P2Y12 receptor–blockade experiments. (**G**) Acute inhibition of microglial P2Y12 receptors prevented neuronal activity–induced increase of microglial process coverage. For statistical data, see the supplementary text for Fig. 4.

(fig. S6A). We observed the fragmentation of mitochondria (Fig. 5A, 74% decrease of individual mitochondrial area, 46% decrease of mitochondrial major axis; $p < 0.001$ for both; $n = 189$ mitochondria) and an almost complete declustering of Kv2.1 proteins in morphologically intact penumbral neurons (Fig. 5B and fig. S6E, from 4 to 0 median clusters/cross-section and from 0.0947 to 0 clusters/μm in control and stroke, respectively, $p < 0.001$; $n = 58$ cells). These morphological changes were accompanied by a robust increase in the microglial process coverage of neuronal cell bodies originating from somatic microglia–neuron junctions in both mice and human postmortem brain tissues (Fig. 5, B to E; mouse: 3.8-fold increase, $p < 0.001$; $n = 30$ neurons; human: 1.5-fold increase, $p = 0.007$; $n = 249$ neurons). Acute intra–cisterna magna administration of the P2Y12 receptor inhibitor PSB or preventing mitochondrial injury by using the mitochondrial ATP–sensitive potassium (KATP) channel opener diazoxide (*38*) completely abolished stroke-induced increases in microglial process coverage around somatic junctions (Fig. 5D, control versus stroke: $p < 0.001$, PSB control versus PSB stroke: $p = 0.792$, diazoxide control versus diazoxide stroke: $p = 0.053$; $n = 140$ neurons). The viability of the examined neurons with increased microglial process coverage was confirmed by normal chromatin structure and membrane integrity (fig. S6, B and C). Transmission electron tomography also confirmed increased microglial process coverage and mitochondrial fragmentation of neurons (Fig. 5C).

To test the impact of P2Y12 receptor–dependent microglial functions on neuronal viability in vivo, we investigated pharmacological inhibition of P2Y12 receptor by injection of PSB intra–cisterna magna before middle cerebral artery occlusion (MCAo). Inhibition of microglial P2Y12 receptor prevented increases in microglial process coverage of neuronal cell bodies in the penumbra and altered functional connectivity in the brain as assessed by a widefield-imaging approach in Thy1-GCaMP6s mice (Fig. 5, F and G). An absence of P2Y12 receptor signaling significantly increased the area of functional disconnection (global connectivity < 0.6) in the ipsilateral hemisphere during ischemia, accompanied by a trend toward elevated neuronal calcium load (Fig. 5F and fig. S6F; $p = 0.0439$; $n = 17$ mice). Seed-based connectivity analysis revealed a significant increase in the contralateral sensory hindlimb area after reperfusion in PSB-treated animals. Moreover, connectivity analysis of 14 functional areas revealed a substantial and widespread increase in connectivity strength in the absence of microglial P2Y12 receptor signaling (Fig. 5G; $p = 0.0077$; $n = 7$ mice).

To examine the effect of P2Y12 receptor inhibition at the single-neuron level in the evolving ischemic penumbra in vivo, we investigated GCaMP6f-injected mice with 2P microscopy. In control mice, neuronal GCaMP6f signal remained unchanged for the first 90 min of reperfusion, whereas blockade of microglial P2Y12 receptors with PSB resulted in a strong elevation in neuronal calcium load (Fig. 5H; $p < 0.0001$; $n = 96$ neurons from 3 mice). This corroborated the findings obtained from the widefield-imaging approach at the cellular level as well. Furthermore, P2Y12 receptor inhibition significantly increased lesion volume at 24 hours reperfusion (Fig. 5I; 54% increase, $p = 0.008$; $n = 20$ mice) and resulted in worse neurological outcome (Fig. 5I; Bederson score, stroke: 1.7 ± 0.26; stroke+PSB: 2.5 ± 0.224, $p = 0.033$; $n = 20$ mice).

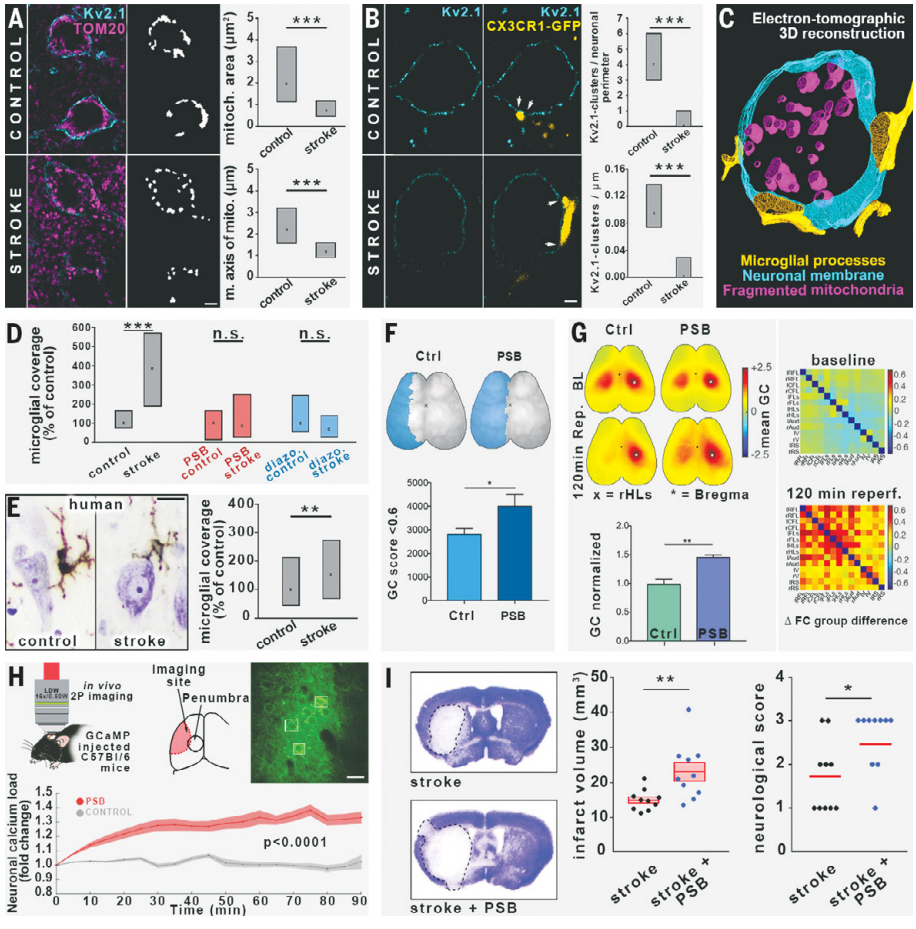

Fig. 5. Microglia protect neurons after acute brain injury in a P2Y12 receptor–dependent manner through altered somatic junctions. (**A**) CLSM images showing that stroke induces the fragmentation of mitochondria (magenta) in neuronal cell bodies (Kv2.1 labeling, cyan) in the penumbra. Mitochondrial area and mitochondrial major axis are both significantly decreased. (**B**) CLSM images of cortical neurons showing that, in parallel with the declustering of Kv2.1-channels (cyan), microglial coverage (yellow) is significantly increased after stroke in the penumbra. (**C**) 3D reconstruction from electron tomographic volume showing elevated microglial coverage and fragmentation of neuronal mitochondria. (**D**) Microglial coverage of neuronal cell bodies is robustly increased after stroke, whereas acute central blockade of P2Y12 receptors or activation of KATP channels completely abolishes the stroke-induced increase of coverage. (**E**) Stroke induces a 1.5-fold increase in somatic microglia coverage of human cortical neurons. (**F**) Topographical maps showing the area of pixels with a global connectivity (GC) score < 0.6 after ischemia. The sum of outlined pixels revealed higher dropdown of GC in PSB-treated animals after stroke. (**G**) Left panel: Topographical maps showing increased region of interest to GC of the contralateral HLs in PSB-treated mice 120 min after stroke. Right panel: Seed-to-seed connectivity is increased in PSB-treated animals after stroke. (**H**) In vivo 2P calcium imaging revealing a significant increase of neuronal calcium load during reperfusion after acute P2Y12 receptor inhibition with PSB. (**I**) Infarct volume is increased after acute central P2Y12 receptor inhibition, which is accompanied by a significantly worse neurological outcome. For statistical data, see the supplementary text for Fig. 5.

To investigate the duration of the PSB effect in vivo, 2-hour-long imaging sessions were performed with 2P microscopy 1 to 3 hours and 24 to 26 hours after intra–cisterna magna PSB injection (n = 173 contacts analyzed from 3 mice). The lifetime of somatic junctions was significantly reduced by up to 3 hours after PSB administration (56.3% of lifetime under baseline conditions, p = 0.0139), whereas there was no effect observed 1 day later (93.8% of lifetime under baseline conditions), suggesting an acute effect of intra–cisterna magna PSB (fig. S6, H and I). The acute effect of PSB was also confirmed by the histological measurements performed 4 hours after MCAo (Fig. 5D). To verify that PSB injected intra–cisterna magna only inhibited microglial P2Y12 receptors, and not those expressed by circulating platelets, we measured ADP-induced platelet activation in plasma samples 1 hour after MCAo, when blood–brain barrier injury is apparent (*37*, *39*, *40*). ADP-induced increases in platelet CD62P were not altered in mice treated with intra–cisterna magna PSB compared with vehicle-treated animals (fig. S5J).

Disintegration of somatic microglia–neuron junctions after neuronal injury triggers increased microglial process coverage of the cell bodies of compromised but potentially viable neurons through P2Y12 receptor and mitochondrial signaling. This could allow the initiation of protective microglial responses that limit brain injury.

Discussion

Here, we describe a form of interaction between microglia and neurons. Under physiological conditions, somatic microglia–neuron junctions were present on most of the neurons in both mice and humans. The junctions appeared to function as communication sites that are rapidly altered in response to brain injury. We propose that microglia constantly monitor neuronal status through these somatic junctions, allowing neuroprotective actions to take place in a targeted manner.

Sites of somatic junctions in neurons were preferentially and repeatedly contacted by microglia. Such interactions had much longer lifetimes compared with the microglial contacts targeting dendrites. In previous studies, the proximity between microglial cell bodies or processes with neuronal somata has been observed in zebrafish and mice (*41*, *42*). However, the formation of direct membrane-to-membrane junctions, the molecular identity of neuronal membranes contacted, activity-dependent recruitment of microglial processes to neuronal cell bodies, the mechanisms of junction formation, and the function of somatic microglia–neuron interactions have not been addressed. Therefore, we took advantage of cutting-edge neuroanatomical approaches and discovered that somatic microglia–neuron junctions are characterized by specific ultrastructural and molecular composition. These morphological and molecular features are absent in perisomatic boutons contacted by microglia, suggesting that the main form of neuronal quality control by microglial processes is not mediated by interactions between microglia and perisomatic axon terminals.

Mitochondria are the primary energy generators in cells, playing fundamental roles in calcium homeostasis, intracellular signaling (*43*, *44*), and neuronal quality control (*45*), as well as in determining cellular fate (*46*). Although neuronal mitochondria are also considered "immunometabolic hubs" involved in antigen presentation and the regulation of innate immune responses (*47*, *48*), changes in mitochondrial function caused by metabolic imbalance, oxidative stress, inflammation, cellular injury, or cell death occur in most neuropathological states (*49*). MAMs are also considered to be key integrators of metabolic and immunological signals, playing a central role in neurodegeneration and cell-fate decisions (*30*, *50*, *51*). Thus, somatic mitochondria and MAMs are ideally positioned to report neuronal status to microglia and to mediate neuronal quality control. Consistent with this, we show that the recruitment of microglial processes to somatic junctions in the vicinity of neuronal mitochondria is linked with mitochondrial activity. This may indicate rapid sensing of mitochondrial activity–associated changes of neurons by microglial processes through the release of ATP and other mediators or the impact of microglia-derived substances on neuronal activity and/or mitochondrial function at somatic junctions. Neurons can execute somatic ATP release through pannexin hemichannels, voltage-dependent anion channels, or activity-dependent vesicle exocytosis (*21*, *22*, *36*). vNUT is known to be responsible for somatic vesicular ATP release in neurons (*34*). In fact, we demonstrated the enrichment of vNUT between neuronal mitochondria and the somatic membranes contacted by microglia and, using time-lapse imaging and HPLC measurements, we confirmed the presence of activity-dependent somatic ATP release from neurons that was blocked by vNUT inhibition. TOM20-positive mitochondria-derived vesicles and other vesicles were also observed within the neuronal cytoplasm at somatic microglia–neuron junctions, together with the enrichment of LAMP1-positive lysosomes, which could, together with the released ATP, provide a constant readout of neuronal activity and mitochondrial function as seen in neurons and other cells (*31*, *52*). The strong enrichment of vNUT in these contacts, the existence of an activity- and vNUT-dependent somatic ATP release, the presence of filamentous cytoplasmatic structures connecting vesicles to the core of the junction, the presence of TOM20 immunogold–positive vesicles within the contacts attached to the neuronal PM, the close association of neuronal lysosomes, and the massive accumulation and nanoscale clustering of exocytosis-promoting Kv2.1 proteins within these contact sites collectively indicate the convergence of multiple parallel vesicular exocytotic pathways at somatic microglia–neuron junctions.

Kv2.1 channels are major regulators of neuronal potassium levels. However, they tend to assemble into discrete clusters on the surface of neurons, where they do not function as ion channels, but rather provide sites for intensive membrane trafficking as exocytotic and endocytotic hubs (*17*, *18*, *53*). Furthermore, Kv2.1 clusters are known to induce stable ER–PM junctions (*53*), anchoring MAMs and mitochondria into these morphofunctional units and providing an ideal site for the release of mitochondria-associated messenger molecules (*31*). The functional importance of these interactions is confirmed by our results showing that Kv2.1 clusters on transfected HEK cells readily induced the formation of microglial process contacts to these clusters, which could not be observed on HEK cells transfected with the dominant-negative mutant Kv2.1. Furthermore, microglial P2Y12 receptor clusters were precisely aligned with neuronal Kv2.1 clusters at somatic junctions.

The activation of P2Y12 receptors was mainly associated with injury or pathological states in previous studies and was considered negligible for physiological microglial surveillance on the basis of ex vivo studies (*54*). Compared with normal extracellular ATP levels in the brain, high levels of ATP (1 mM) were shown to induce P2Y12 receptor–dependent microglial recruitment, similar to that seen during microglial phagocytosis or in models of synaptic plasticity, whereas microglial surveillance is considered to be P2Y12 receptor independent (*54*, *55*). Our in vivo results refine this view and highlight the importance of the compartment-dependent effects of P2Y12 receptor on microglial process responses: PSB0739 significantly reduced somatic junction lifetime but did not affect the lifetime of dendritic microglia–neuron contacts, whereas it abolished microglial reactions to altered neuronal activity, confirming P2Y12 receptor dependence of microglial actions under physiological conditions. Furthermore, neuronal mitochondrial activity was also linked with physiological microglial P2Y12 receptor activity at these junctions. It is also possible that P2Y12 receptor–mediated actions are more important for sustaining than for forming somatic junctions during the communication between neuronal somata and microglial processes. The contact-dependent clustering of P2Y12 receptors further confirms their involvement in physiological microglia–neuron interactions at somatic

junctions. Blockade of microglial P2Y12 receptor left cortical synapse numbers completely unchanged and contact-dependent nanoclustering of microglial P2Y12 receptors was not seen when microglia contacted synaptic boutons. Thus, microglia–neuron interactions at these sites are not only P2Y12 receptor dependent, they are also fundamentally different from those seen at synapses.

The failure of most neuroprotection trials in stroke and other brain diseases strongly indicates the importance of understanding the complexity of pathophysiological processes, including microglial actions. Potentially salvageable neurons around the infarct core may show metabolic activity up to 6 to 17 hours after stroke in patients and experimental animals (*56*, *57*). Here, Kv2.1 declustering was observed in compromised neurons of the penumbra as early as 4 hours after brain injury, which paralleled mitochondrial fragmentation in neurons and increased microglial process coverage around somatic microglia–neuron junctions. Thus, P2Y12 receptor–dependent microglial actions protect neurons, whereas blockade of microglial P2Y12 receptor signaling alone impaired cortical network function and increased calcium load and the area of ischemia-induced disconnection within 2 hours after stroke (a clinically relevant time window). This increase in brain injury was similar to that seen after the complete and selective elimination of microglia (*37*). These protective microglia- and P2Y12 receptor–mediated effects were linked with mitochondrial actions initiated upon neuronal injury because the diazoxide (a KATP channel opener)–abolished increases in microglial process coverage of neurons after stroke were similar to those seen after blockade of P2Y12 receptor signaling.

All of these results unequivocally indicate that microglia continuously monitor neuronal status through somatic junctions, rapidly responding to neuronal changes and initiating neuroprotective actions.

We propose that healthy neurons may constitutively release ATP and other signaling molecules at these junctions, communicating their "well-being" to microglia. In turn, disintegration of these specialized morphofunctional hubs caused by excitotoxicity, energy depletion, or other noxious stimuli may trigger rapid and inherently protective microglial responses, leading to the restoration of neuronal function or the isolation and phagocytosis of dying neurons in case terminal neuronal injury occurs (*55*). Along with P2Y12 receptor–mediated microglial process recruitment, it is likely that a broad range of signals is integrated at somatic microglial junctions and, through these, microglia may sense products of neuronal exocytosis and changes in the cell membrane (e.g. apoptotic signals) and alter the duration of physical contact or initiate phagocytosis. The most important open research areas include the clarification of additional signaling mechanisms (vesicular and nonvesicular) involved in neuron-to-microglia communication at these junctions and the mechanisms of microglial neuroprotection (e.g. regulation of neuronal ion fluxes, neuronal calcium dynamics, or the metabolism of neuronal mitochondria). Because the role of microglia–neuron somatic junctions in most brain diseases is completely unknown, microglia–neuron interactions through these sites may differ in different forms of acute and chronic neuropathologies.

REFERENCES AND NOTES

1. M. S. Thion, F. Ginhoux, S. Garel, *Science* **362**, 185–189 (2018).
2. K. Kierdorf, M. Prinz, *J. Clin. Invest.* **127**, 3201–3209 (2017).
3. M. W. Salter, B. Stevens, *Nat. Med.* **23**, 1018–1027 (2017).
4. W. M. Song, M. Colonna, *Nat. Immunol.* **19**, 1048–1058 (2018).
5. D. Davalos *et al*., *Nat. Neurosci.* **8**, 752–758 (2005).
6. A. Nimmerjahn, F. Kirchhoff, F. Helmchen, *Science* **308**, 1314–1318 (2005).
7. Y. Wu, L. Dissing-Olesen, B. A. MacVicar, B. Stevens, *Trends Immunol.* **36**, 605–613 (2015).
8. L. Weinhard *et al*., *Nat. Commun.* **9**, 1228 (2018).
9. J.-M. Cioni, M. Koppers, C. E. Holt, *Curr. Opin. Neurobiol.* **51**, 86–94 (2018).
10. T. Misgeld, T. L. Schwarz, *Neuron* **96**, 651–666 (2017).
11. M. Terenzio, G. Schiavo, M. Fainzilber, *Neuron* **96**, 667–679 (2017).
12. J. Aarum, K. Sandberg, S. L. B. Haeberlein, M. A. A. Persson, *Proc. Natl. Acad. Sci. U.S.A.* **100**, 15983–15988 (2003).
13. M. Ueno *et al*., *Nat. Neurosci.* **16**, 543–551 (2013).
14. J. L. Marín-Teva, M. A. Cuadros, D. Martín-Oliva, J. Navascués, *Neuron Glia Biol.* **7**, 25–40 (2011).
15. A. Sierra *et al*., *Neural Plast.* **2014**, 610343 (2014).
16. H. Wake, A. J. Moorhouse, S. Jinno, S. Kohsaka, J. Nabekura, *J. Neurosci.* **29**, 3974–3980 (2009).
17. E. Deutsch *et al*., *Mol. Biol. Cell* **23**, 2917–2929 (2012).
18. L. Feinshreiber, D. Singer-Lahat, U. Ashery, I. Lotan, *Ann. N. Y. Acad. Sci.* **1152**, 87–92 (2009).
19. M. Kirmiz, N. C. Vierra, S. Palacio, J. S. Trimmer, *J. Neurosci.* **38**, 7562–7584 (2018).
20. B. Jiang, X. Sun, K. Cao, R. Wang, *Mol. Cell. Biochem.* **238**, 69–79 (2002).
21. A. Menéndez-Méndez *et al*., *Front. Pharmacol.* **8**, 951 (2017).
22. R. D. Fields, *Semin. Cell Dev. Biol.* **22**, 214–219 (2011).
23. S. E. Haynes *et al*., *Nat. Neurosci.* **9**, 1512–1519 (2006).
24. Y. Zhang *et al*., *J. Neurosci.* **34**, 11929–11947 (2014).
25. O. Butovsky *et al*., *Nat. Neurosci.* **17**, 131–143 (2014).
26. B. Dudok *et al*., *Nat. Neurosci.* **18**, 75–86 (2015).
27. I. D. Campbell, M. J. Humphries, *Cold Spring Harb. Perspect. Biol.* **3**, a004994 (2011).
28. H. Akiyama, P. L. McGeer, *J. Neuroimmunol.* **30**, 81–93 (1990).
29. F. E. McCann *et al*., *J. Immunol.* **170**, 2862–2870 (2003).
30. G. Csordás, D. Weaver, G. Hajnóczky, *Trends Cell Biol.* **28**, 523–540 (2018).
31. A. Sugiura, G.-L. McLelland, E. A. Fon, H. M. McBride, *EMBO J.* **33**, 2142–2156 (2014).
32. V. Soubannier *et al*., *Curr. Biol.* **22**, 135–141 (2012).
33. T. Ho *et al*., *Front. Cell. Neurosci.* **9**, 389 (2015).
34. Y. Moriyama, M. Hiasa, S. Sakamoto, H. Omote, M. Nomura, *Purinergic Signal.* **13**, 387–404 (2017).
35. A. M. Brennan, J. A. Connor, C. W. Shuttleworth, *J. Cereb. Blood Flow Metab.* **26**, 1389–1406 (2006).
36. X. Zhang, Y. Chen, C. Wang, L.-Y. M. Huang, *Proc. Natl. Acad. Sci. U.S.A.* **104**, 9864–9869 (2007).
37. G. Szalay *et al*., *Nat. Commun.* **7**, 11499 (2016).
38. J. O. Onukwufor, D. Stevens, C. Kamunde, *J. Exp. Biol.* **219**, 2743–2751 (2016).
39. F. Orsini *et al*., *Arterioscler. Thromb. Vasc. Biol.* **38**, 2678–2690 (2018).
40. K. Bekő *et al*., *J. Thromb. Haemost.* **15**, 1223–1235 (2017).
41. Y. Li, X.-F. Du, C.-S. Liu, Z.-L. Wen, J.-L. Du, *Dev. Cell* **23**, 1189–1202 (2012).
42. R. D. Stowell *et al*., *Dev. Neurobiol.* **78**, 627–644 (2018).
43. C. N. Hall, M. C. Klein-Flügge, C. Howarth, D. Attwell, *J. Neurosci.* **32**, 8940–8951 (2012).
44. N. S. Chandel, *BMC Biol.* **12**, 34 (2014).
45. E. I. Rugarli, T. Langer, *EMBO J.* **31**, 1336–1349 (2012).
46. A. Kasahara, L. Scorrano, *Trends Cell Biol.* **24**, 761–770 (2014).
47. D. Arnoult, F. Soares, I. Tattoli, S. E. Girardin, *EMBO Rep.* **12**, 901–910 (2011).
48. G. R. Bantug *et al*., *Immunity* **48**, 542–555.e6 (2018).
49. A. U. Joshi, D. Mochly-Rosen, *Pharmacol. Res.* **138**, 2–15 (2018).
50. J. Rieusset, *Biochem. Biophys. Res. Commun.* **500**, 35–44 (2018).
51. R. Bravo-Sagua *et al*., *Curr. Mol. Med.* **13**, 317–329 (2013).
52. G.-L. McLelland, S. A. Lee, H. M. McBride, E. A. Fon, *J. Cell Biol.* **214**, 275–291 (2016).
53. P. D. Fox *et al*., *J. Cell Sci.* **128**, 2096–2105 (2015).
54. C. Madry *et al*., *Neuron* **97**, 299–312.e6 (2018).
55. R. Fekete *et al*., *Acta Neuropathol.* **136**, 461–482 (2018).
56. G. Marchal *et al*., *Stroke* **27**, 599–606 (1996).
57. J. C. Baron, M. E. Moseley, *J. Stroke Cerebrovasc. Dis.* **9**, 15–20 (2000).

ACKNOWLEDGMENTS

We thank L. Barna and the Nikon Imaging Center at the Institute of Experimental Medicine (IEM) for kindly providing microscopy support, D. Mastronarde at MCDB for his continuous help with IMOD software, and S. Kovács from ETH Zurich for scripting analytic tools. We are also grateful to N. Hájos (IEM), Z. Nusser (IEM), and J. Trimmer (University of California, Davis) for their support and useful comments. We thank the Department of Pathology, St. Borbála Hospital, Tatabánya, and the Human Brain Research Lab at the IEM for providing human brain tissue and D. Gali-Györkei and R. Rácz for excellent technical assistance. We also thank Plexxikon for providing PLX5622 and Deltagen for the donation of P2Y12 receptor$^{-/-}$ mice. **Funding:** This work was supported by a Momentum Research Grant from the Hungarian Academy of Sciences (LP2016-4/2016 to A.D.) and ERC-CoG 724994 (A.D.), a János Bolyai Research Scholarship of the Hungarian Academy of Sciences (C.C., and N.L), and grants UNKP-19-3-I (B.P.) and UNKP-19-4 (C.C.) from the New National Excellence Program of the Ministry for Innovation and Technology. Additionally, this work was funded by H2020-ITN-2018-813294-ENTRAIN (A.D.), the Hungarian Academy of Sciences (G.T.), the National Research, Development and Innovation Office of Hungary (GINOP-2.3.2-15-2016-00018, VKSZ-14-1-2015-0155, G.T.), the Ministry of Human Capacities, Hungary (20391-3/2018/FEKUSTRAT, G.T.), the German Research Foundation (FOR 2879), and ERC-StG 802305 to A.L. I.K. was supported by a Momentum Research Grant from the Hungarian Academy of Sciences (LP2013-54), the Hungarian Scientific Research Fund (OTKA, K 116915), and the National Research, Development and Innovation Office of Hungary (VKSZ_14-1-2015-0155). M.M.T. was supported by National Institutes of Health grant R01GM109888. B.S. and Z.M. were supported by the National Research, Development and Innovation Office of Hungary (K116654 to B.S. and K125436 to Z.M.) and by the National Brain Research Program (2017-1.2.1-NKP-2017-00002). T.H. was supported by the Hungarian Brain Research Program (1.2.1-NKP-2017-00002). G.M. was supported by Hungarian Scientific Research Fund (OTKA, K128863). L.C. was supported by the National Research, Development and Innovation Fund (GINOP-2.3.2-15-2016-00048-Stay Alive). R.S. was supported by Hungarian Scientific Research Fund (OTKA, K 129047). This work was also supported by EFOP-3.6.3-VEKOP-16-2017-00009 from Semmelweis University. **Author contributions:** The project was conceived by C.C., B.P., and A.D.. Surgery was performed by N.L. and A.D. Two-photon imaging was performed by R.F. Immunohistochemistry and light microscopy were performed by C.C., B.P., A.D., B.O., A.D.S., and E.S. STORM microscopy was performed by B.O. Electron microscopy was performed by C.C., B.P., E.S., and A.D.S. Electron tomography was performed by C.C. and B.P. In vitro NADH imaging was performed by G.M. under the supervision of G.T. Plasmid engineering and in utero electroporation were performed by Z. L. and Z. I. L. In vitro cell culture transfection and experiments were performed by Z.K., K.T., and Z.I.L. Virus injection was performed by R.F. and B.M. Widefield calcium imaging was performed by S.H. under the supervision of A.L. HPLC measurements were performed by M.B. under the supervision of B.S. Data were analyzed by C.C., B.P., B.O., G.M., S.H., N.L., A.D.S., K.U., A.L., and A.D. Critically important clinical and neuropathological data and materials were contributed by L.C.,

T.H., Z.M. G.S., M.M.T., and F.E. The laser-optical setup for dual wavelength in vitro 2P measurements was optimized by R.S. Resources were provided and essential intellectual contributions were made by I.K., G.T., and A.L., who also revised the manuscript. Funding was obtained and the project supervised by A.D. The paper was written by C.C., B.P., and A.D. with input from all authors. **Competing interests:** The authors declare no competing interests. **Data and materials availability:** PLX5622 was obtained under a material transfer agreement with Plexxikon (Berkeley, CA). All data are available in the main text or the supplementary materials.

SUPPLEMENTARY MATERIALS

12 April 2019; resubmitted 14 October 2019
Accepted 3 December 2019
Published online 12 December 2019
10.1126/science.aax6752

Science

Microglia monitor and protect neuronal function through specialized somatic purinergic junctions

Csaba CserépBalázs PósfaiNikolett LénártRebeka FeketeZsófia I. LászlóZsolt LeleBarbara OrsolitsGábor MolnárSteffanie HeindlAnett D. SchwarczKatinka UjváriZsuzsanna KörnyeiKrisztina TóthEszter SzabaditsBeáta SperlághMária BaranyiLászló CsibaTibor HortobágyiZsófia MaglóczkyBernadett MartineczGábor SzabóFerenc ErdélyiRóbert Szip#csMichael M. TamkunBenno GesierichMarco DueringIstván KatonaArthur LieszGábor TamásÁdám Dénes

Science, 367 (6477), • DOI: 10.1126/science.aax6752

Microglia take control

Changes in the activity of microglia, the primary immune cells of the central nervous system, are linked with major human diseases, including stroke, epilepsy, psychiatric disorders, and neurodegeneration. Cserép *et al.* identified a specialized morphofunctional communication site between microglial processes and neuronal cell bodies in the mouse and the human brain (see the Perspective by Nimmerjahn). These junctions are formed at specific areas of the neuronal somatic membranes and possess a distinctive nanoarchitecture and specialized molecular composition linked to mitochondrial signaling. The junctions appear to provide a major site for microglia-neuron communication and may help to mediate the neuroprotective effects of microglia after acute brain injury.

Science, this issue p. 528; see also p. 510

Science (ISSN 1095-9203) is published by the American Association for the Advancement of Science. 1200 New York Avenue NW, Washington, DC 20005. The title *Science* is a registered trademark of AAAS.